PERGAMON

International Journal of Solids and Structures 36 (1999) 3239–3252

INTERNATIONAL JOURNAL OF SOLIDS and STRUCTURES

A boundary element application for mixed mode loading idealized sawtooth fracture surface

Lih-Jier Young*, Yeong-Pei Tsai

Department of Applied Mathematics, Chung-Hua University, Hsin-Chu, Taiwan 30067, People's Republic of China

Received 16 October 1997; in revised form 13 April 1998

Abstract

In this paper, a 2-D elastic-plastic BEM formulation predicting the reduced mode II and the enhanced mode I stress intensity factors are presented. The dilatant boundary conditions (DBC) are assumed to be idealized uniform sawtooth crack surfaces and an effective Coulomb sliding law. Three types of crack face boundary conditions, i.e. (1) BEM sawtooth model-elastic center crack tip; (2) BEM sawtooth model-plastic center crack tip; and (3) BEM sawtooth model-edge crack with asperity wear are presented. The model is developed to attempt to describe experimentally observed non-monotonic, non-linear dependence of shear crack behavior on applied shear stress, superimposed tensile stress, and crack length. The asperity sliding is governed by Coulomb's law of friction applied on the inclined asperity surface which has coefficient of friction μ. The traction and displacement Green's functions which derive from Navier's equations are obtained as well as the governing boundary integral equations for an infinite elastic medium. Accuracy test is performed by comparison stress intensity factors of the BEM model with analytical solutions of the elastic center crack tip. The numerical results show the potential application of the BEM model to investigate the effect of mixed mode loading problems with various boundary conditions and physical interactions.

1. Introduction

The general picture of the effects of fracture surface interference on shear mode (mode II and mode III) of crack growth is one of interlocking asperities that both resist shear displacements are forced to ride up on one another. Thus, the driving force for shear crack growth extension is decreased by asperity shielding and induced mode I opening may be sufficient to cause crack extension in a macroscopically shear mode of crack growth. Boundary element methods is used to model the complex resistance to the applied field to define an effective driving force for crack growth. The fracture surface is described in the model using such parameters as asperity height,

* Corresponding author. Fax: 00886 3 5373 771.

0020–7683/99/$ - see front matter
PII: S0020–7683(98)00147–4

interaction distance, slope, and several empirical asperity wear criteria. The model is developed to describe the observed non-monotonic, non-linear dependence of shear crack growth on applied shear stress, superimposed tensile stress, and cyclic load history.

2. BEM sawtooth model-elastic center crack tip

The physical asperity interaction model is described schematically in Fig. 1, which illustrates a representative segment of displaced crack surfaces. The equation

$$\tau_a = \mu\sigma_a \tag{1}$$

states that asperity sliding is governed by Coulomb's law of friction, with coefficient of friction μ. In order to implement this in the BEM formulation without modeling the actual sawtooth surface a macroscopic crack plane is taken parallel to the midplane of the perfectly meshed sawtooth surface and standard stress transformation, i.e.

$$\sigma_c = \sigma_a \cos(\alpha) - \tau_a \sin(\alpha), \tag{2}$$

$$\tau_c = \tau_a \cos(\alpha) + \sigma_a \sin(\alpha) \tag{3}$$

performed to obtain an effective Coulomb sliding law on that plane. This yields the equation

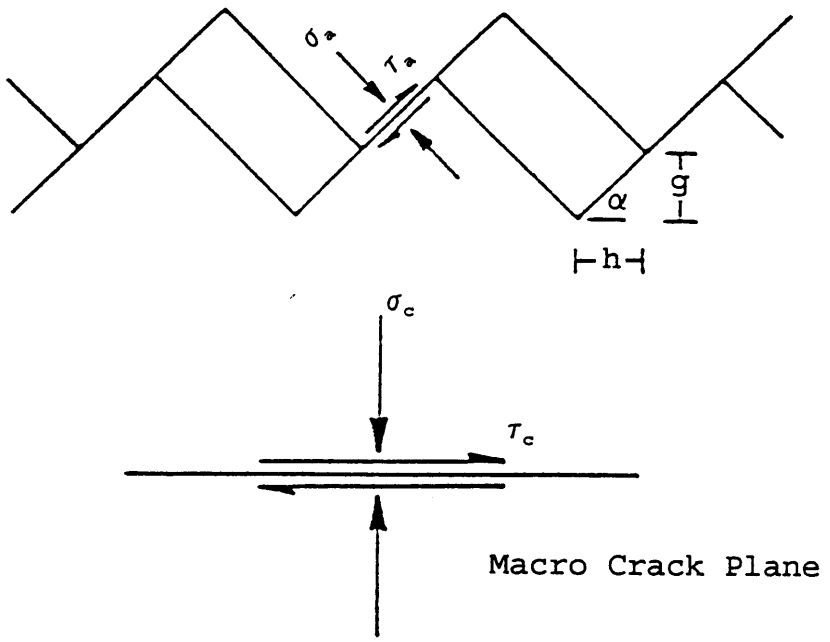

Fig. 1. Two dimensional geometry of idealized sawtooth contact with asperity angle α, crack opening displacement g, crack sliding displacement h, coefficient of friction μ and effective coefficient of friction Γ.

$$\tau_c = \Gamma \sigma_c \tag{4}$$

where Γ, the effective coefficient of friction, is defined in as

$$\Gamma = \frac{\mu + \tan(\alpha)}{1 - \mu \tan(\alpha)}, \tag{5}$$

and α is the asperity angle. The assumption of rigid body asperity sliding yields an induced opening proportional to the sliding as expressed by $g = h\tan(\alpha)$, where g is the crack opening displacement, COD, and h is the crack sliding displacement, CSD, both referring to the macroscopic crack plane. Since g and h will vary along the length of the crack, the asperities may only be considered to be locally rigid in so far as they maintain planar surfaces. However, they must be considered deformable in bulk to accommodate the varying g and h.

The first step in the BEM solution is to divide the cracked body into two bodies along the plane of the crack, referred to below as the interface. The interaction between the two bodies is included through boundary conditions relating the displacements and stresses on either side of the interface. At points on the uncracked portion of the interface the 2 displacement components and the 2 stress components must be continuous. At points on the cracked portion of the interface the stresses are continuous (2 conditions) and are related by eqn (4) (1 condition), and $g = h\tan(\alpha)$ after g and h are expressed in terms of the displacements on opposite crack face. Thus, at each pair of points on the interface we have four conditions involving eight quantities. Four of those are eliminated algebraically using the boundary conditions, thus, leaving four unknowns at each point. Two coupled boundary integral equations, written as a function of position on the boundary of a body, enforce all of the field equations of elasticity for that body. The two equations for each of the two artificially divided bodies are applied to each discretized point on the interface, thus giving four equations and four unknowns at each pair of interface points. If the boundary of either of the artificially divided bodies consists of other than the common interface, then at each of these boundary points there are four boundary quantities to be accounted for. The only condition we have used on these external boundaries has been prescribed stress, thus leaving the two displacements as unknowns, with two equations provided by that body's two boundary integral equations. The case of a crack lying on the interface between dissimilar materials is obtained from the above formulation simply by making the elastic constants in two bodies different.

The BEM consists of the discretization of the boundary surfaces and the numerical approximation of the boundary quantities in the set of equations obtained from the boundary integrals in Young (1994) as described above. We model the boundary, using straight-line elements, centered about nodes at which the integral equations are applied in Young (1994). For straight boundary this introduces no approximations. We assume that the stress and displacement are constant throughout each straight-line element. This approximation allows their removal from the integral, resulting in integrals of the known 2D Green's function which have been evaluated in closed form in Young (1994). The final result is a system of simultaneous linear algebraic equations for the unknowns nodal displacements and stresses. After the system is solved the crack tip stress intensity factors (SIF's) are calculated by fitting the calculated COD or CSD to the standard square root form at an elastic crack tip.

The results shown here are for a finite length crack (10 mm) either in an infinite homogeneous body with shear modulus G and Poisson's ratio v. The applied loading is uniform remote tensile

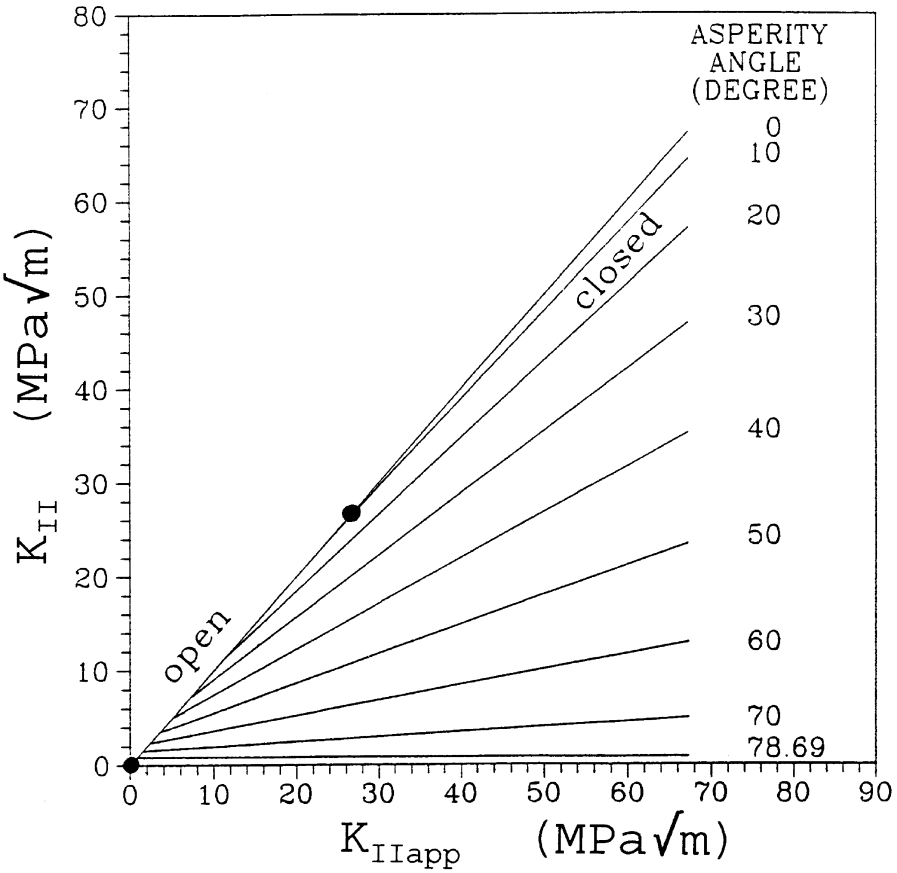

Fig. 2. K_{II} vs K_{IIapp} for various values of asperity angle α ($G = 80{,}000$ MPa, $v = 0.3$, $N = 30$ MPa, $\mu = 0.2$, $2a = 10$ mm).

stress N and shear stress S. The effective (applied minus resistance) mode II shear SIF and the total (induced plus applied) mode I SIF for a homogeneous aluminum medium are denoted by K_{II} and K_I in Figs 2 and 3. They are plotted vs the applied shear SIF K_{IIapp}, which is calculated using S in the open crack SIF solution. K_{Iapp} is found in the same way using N. Each curve in Figs 2 and 3 is for a single value asperity angle α and $N = 30$ MPa and $\mu = 0.2$ which gives $\Gamma = 1.250$. Here K_{II} and K_I refer to the actual or effective mode II and I SIF, respectively. Thinking of N as being applied first and then S being increased from zero there is a range of applied shear for which the crack surfaces are not in contact and the applied and actual K_{II}s are equal. This range is denoted by 'OPEN' on $\alpha = 10^\circ$ curves. But, when S is large enough to make $K_{IIapp} = K_{IIclosure} = K_{Iapp}\cot(\alpha)$ the asperities come into contact, and as S increases further the model goes into effect and shielding occurs. This portion is denoted by 'CLOSED' on $\alpha = 10^\circ$ curves. The results of both 'OPEN' and 'CLOSED' portions are linear. In addition, the ratio of the mode II effective SIF to the mode I induced SIF is constant and equal to $\cot(\alpha)$ in the 'CLOSED' portion. The value of K_{IIapp} at which the crack faces touch and shielding begins to decrease as α increases, and can be identified in Figs

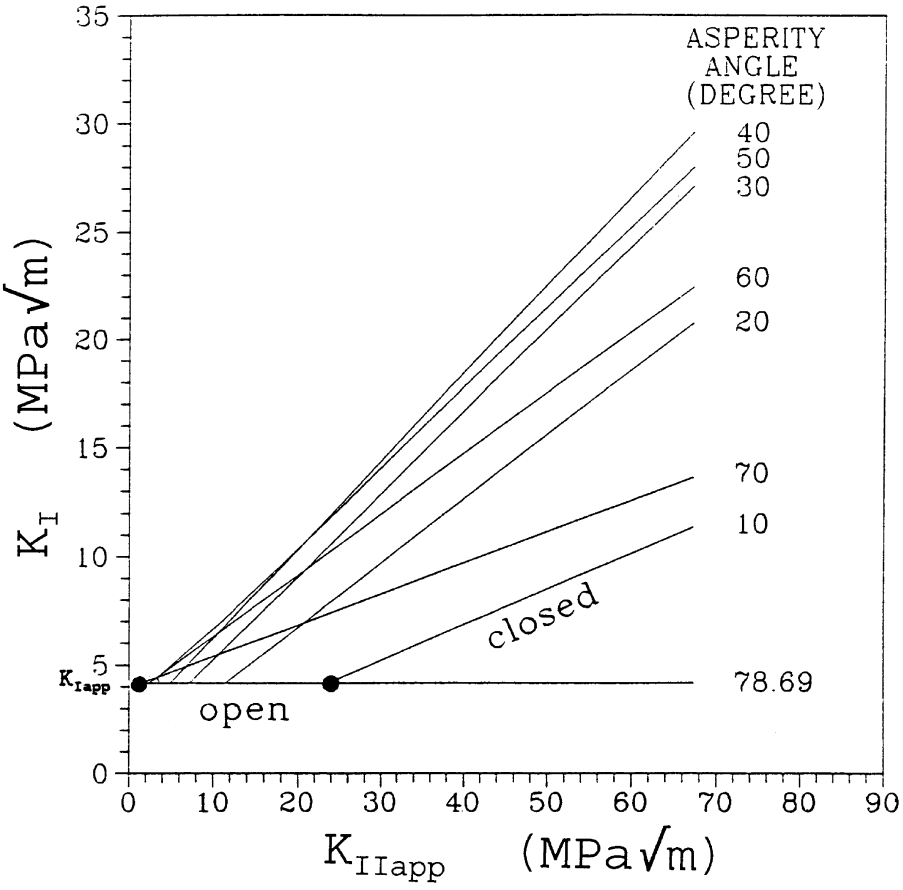

Fig. 3. K_I vs K_{IIapp} for various values of asperity angle α ($G = 80{,}000$ MPa, $v = 0.3$, $N = 30$ MPa, $\mu = 0.2$, $2a = 10$ mm).

2 and 3 as the intersection of the various lines with the $K_{II} = K_{IIapp}$ line of unit slope and the $K_I = K_{Iapp}$ = constant horizontal line, respectively. While the slopes of the K_{II} lines decrease with α everywhere, the slopes of the K_I lines increase with α from 0° to 45°, reach a maximum and then decrease all the way to $K_I = K_{Iapp}$ where $\alpha = 78.69^\circ$. If $\alpha > 78.69^\circ$ the effective coefficient of friction Γ is infinite and the crack is locked. Also the values $K_I = K_{Iapp}$ and $K_{II} = K_{IIclosure}$ are locked in.

Figure 4 is an example of a parameter study with respect to the micro-mechanical variables. K_{II} and K_I are plotted vs asperity angle α for three different values of coefficient of friction μ, keeping N and S fixed. The plots cover the entire physical range of α. Since μ represents the coefficient of friction for a smooth faceted asperity surface, zero to one is a fairly wide range for μ as well. Focusing on the $\mu = 1.0$ curves, the crack is open if $\alpha < 13^\circ$, closed if $\alpha > 13^\circ$. The open/closed transition depends on N and S only. If $\alpha > 45^\circ$ the effective coefficient of friction Γ is infinite and the crack is locked. The value of the locked K_I is K_{Iapp} and the value of the locked K_{II} depends on the amount sliding which occurs before the contact occurs, and happens to be equal to K_{Iapp} in this case because the locking angle for $\mu = 1.0$ is 45°. The $\mu = 0.0$ and 0.2 curves may be interpreted similarly. The results show that as α increases K_I increases for a while, as expected from the

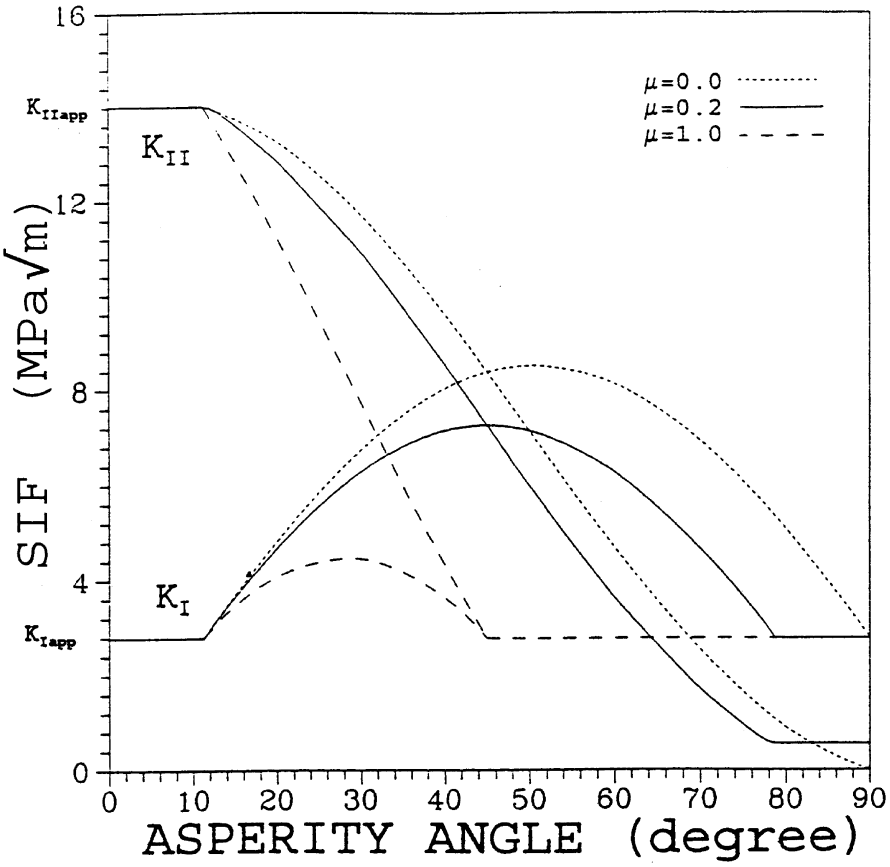

Fig. 4. Stress intensity factor vs asperity slope for various coefficients of friction of μ ($G = 80{,}000$ MPa, $v = 0.3$, $N = 30$ MPa, $S = 130$ MPa, $2a = 10$ mm).

imposed COD/CSD relationships. However, at some critical α the counteracting effect of greater normal contact stress σ_c and greater Γ, and hence greater frictional stress τ_c, takes over and K_I begins to decrease with increasing α.

3. BEM sawtooth model-plastic center crack tip

The formulation for small-scale plasticity at the crack tip is based on a re-formulation of the Dugdale strip yielding model in Dugdale (1960) to the mixed mode open crack case, in which the normal and shear stresses in the plastic zone have the same ratio as the applied normal and shear stresses, but are both functions of the uni-axial tensile yield stress and the applied stresses in Becker and Gross (1989). The case of the mixed mode Dugdale non-interfering crack problem is shown

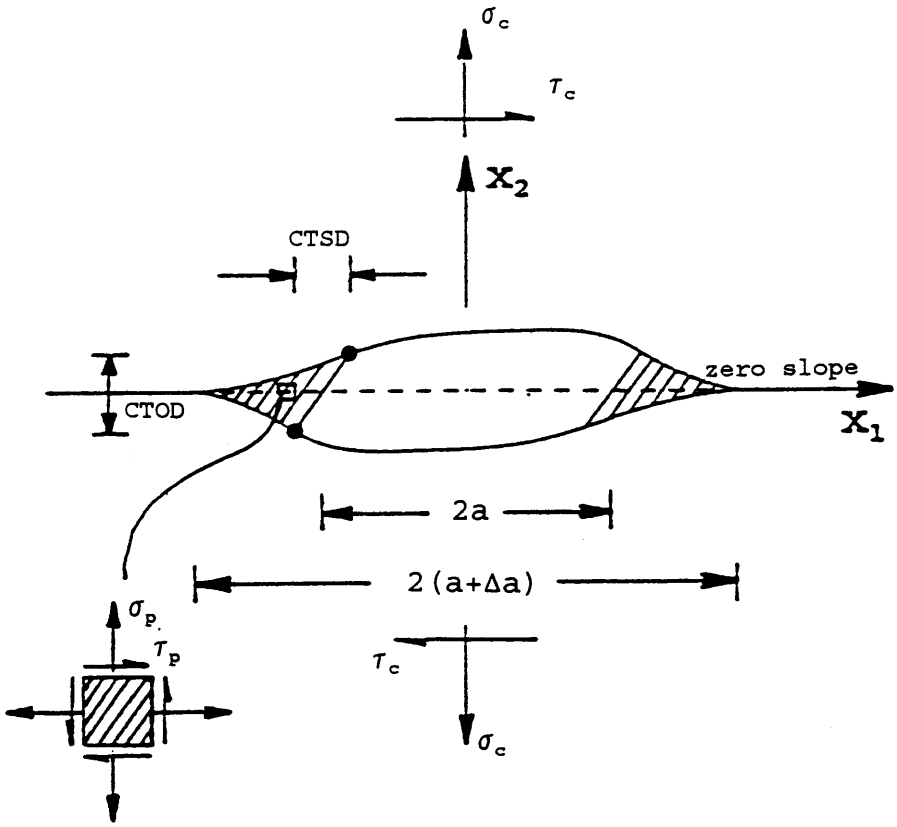

Fig. 5. Mixed mode Dugdale crack problem.

in Fig. 5. In the single mode case the stress is either the tensile yield stress or the shear yield stress. The length of the mixed mode plastic zone is also given in terms of the same quantities, just as in the single mode open crack Dugdale case. We adapt these ideas to our numerical formulation by replacing the applied loading with effective SIFs and unknown plastic zone length in terms of the unknown effective mode I and II SIFs. We solve the non-linear problem directly for two effective SIFs using Newton's method subject to the conditions of zero slope in the COD and CSD at the end of the plastic zone in Young (1994). For a given iteration on the effective K_I and K_{II}, the associated plastic zone stresses and plastic zone length are calculated from the modified Dugdale (1960) in terms of K_I and K_{II}. These plastic zone stresses are used in prescribed stress boundary conditions for the newly formulated plastic zone interface region in a revised BEM code and the COD, CSD and their slopes at the end of the plastic zone are calculated. These are then put into the 2D Newton's method formulas for the next iterated values of K_I and K_{II}. The iteration is stopped when the difference between two subsequent guesses reaches some prescribed small number.

In order to focus only on the DBC interaction all results in Figs 6, 7 and 8 are for pure shear loading, $N = 0$ for a finite length crack (10 mm). Figures 6 and 7 show the analogous results of

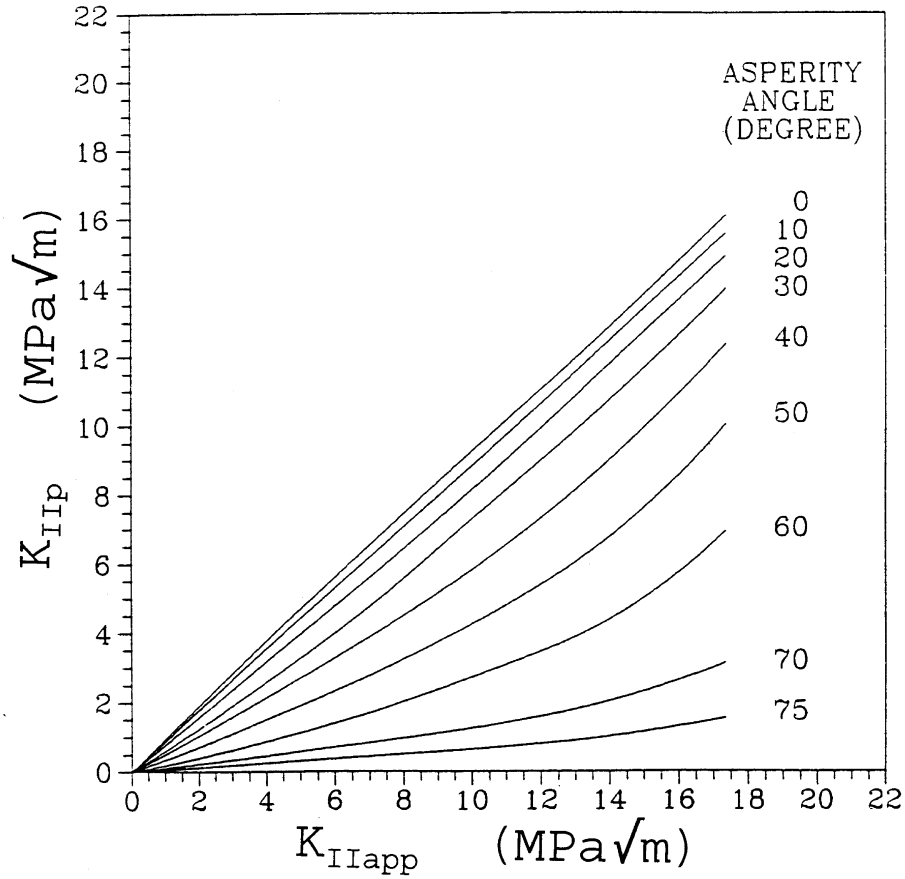

Fig. 6. K_{II} vs K_{IIapp} for various values of asperity angle α ($G = 80{,}000$ MPa, $\nu = 0.3$, $N = 0$ MPa, $\mu = 0.2$, $2a = 10$ mm, $\sigma_y = 300$ MPa).

elastic DBC boundary conditions (Figs 2 and 3) for plastic DBC boundary conditions. The results are for various values of asperity angle α at fixed coefficient of friction, $\mu = 0.2$. They also show that the K_{IIp} vs K_{IIapp} curves decrease monotonically in slope and magnitude as α increases in slope and magnitude as K_{IIapp} increases, not present in the elastic case, indicating that with plasticity at the tip the effects of the roughness diminish with increased applied shear. Experimental evidence in the two papers by Tong (1995) can also support these observations. The K_{Ip} vs K_{IIapp} curves, on the other hand, show that K_{Ip} reaches a maximum at some critical value of K_{IIapp}, which increases monotonically with α, and then decreases steadily from that maximum with increased applied shear. While out of the range of the plots shown, the curves for $\alpha = 60^\circ$ and greater do reach a maximum at increasingly larger values of K_{IIapp}. The magnitude of the maximum value of K_{Ip} with respect to K_{IIapp} increases with α up to some critical value of α and then decreases with α until α reaches the locking value. This critical value of α increases with K_{IIapp} and for the K_{IIapp} range shown varies between $\alpha = 40^\circ$ and 60°.

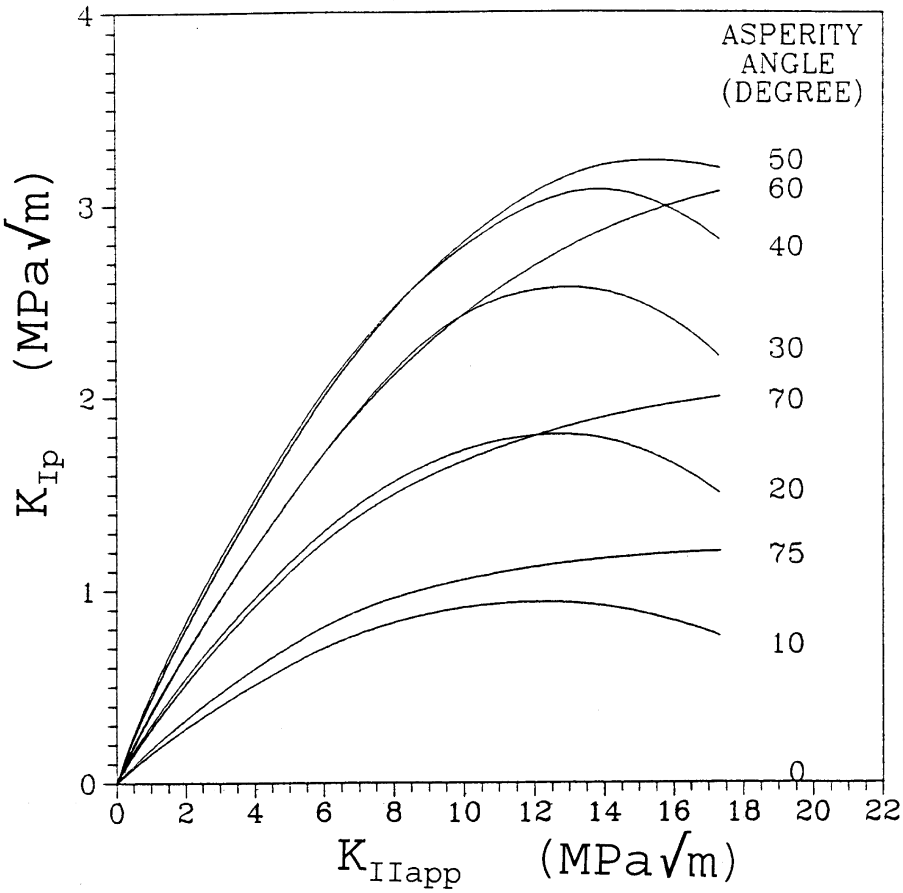

Fig. 7. K_I vs K_{IIapp} for various values of asperity angle α ($G = 80{,}000$ MPa, $\nu = 0.3$, $N = 0$ MPa, $\mu = 0.2$, $2a = 10$ mm, $\sigma_y = 300$ MPa).

Also it is observed that, at increasingly large values of K_{IIapp} as α increases, K_{Ip} will eventually return to zero, indicating zero plastic crack tip opening displacement.

Figure 8 is a plot of elastic, plastic and critical K_{II} and K_I vs asperity angle α for $\mu = 0.2$. The applied shear S and normal stress N are 100 MPa and 20 MPa, respectively, and are held fixed. The critical stress intensity factors, K_{ce} and K_{cp} are the mode I tensile Ks on the plane at the crack tip for which the tensile stress is maximum. This plane is never the original crack plane if both K_I and K_{II} are non-zero. In the maximum tensile stress mixed mode fracture propagation criterion proposed by Erdogan and Shih (1963) it is K_c which controls the onset of crack growth and growth occurs in the plane of maximum tensile stress. In Fig. 8 the critical angle between no contact or contact is 13° and the critical angle for locking is 78.69°. Both of them are the same as described in the elastic case of Fig. 4. Also the elastic K_{Ie} is always larger than plastic K_{Ip}. However the plastic K_{IIp} and K_{cp} are always larger than elastic K_{IIe} and K_{ce}. It is worth mentioning that the elastic Ks and the corresponding plastic Ks should overlap each other when there is no contact

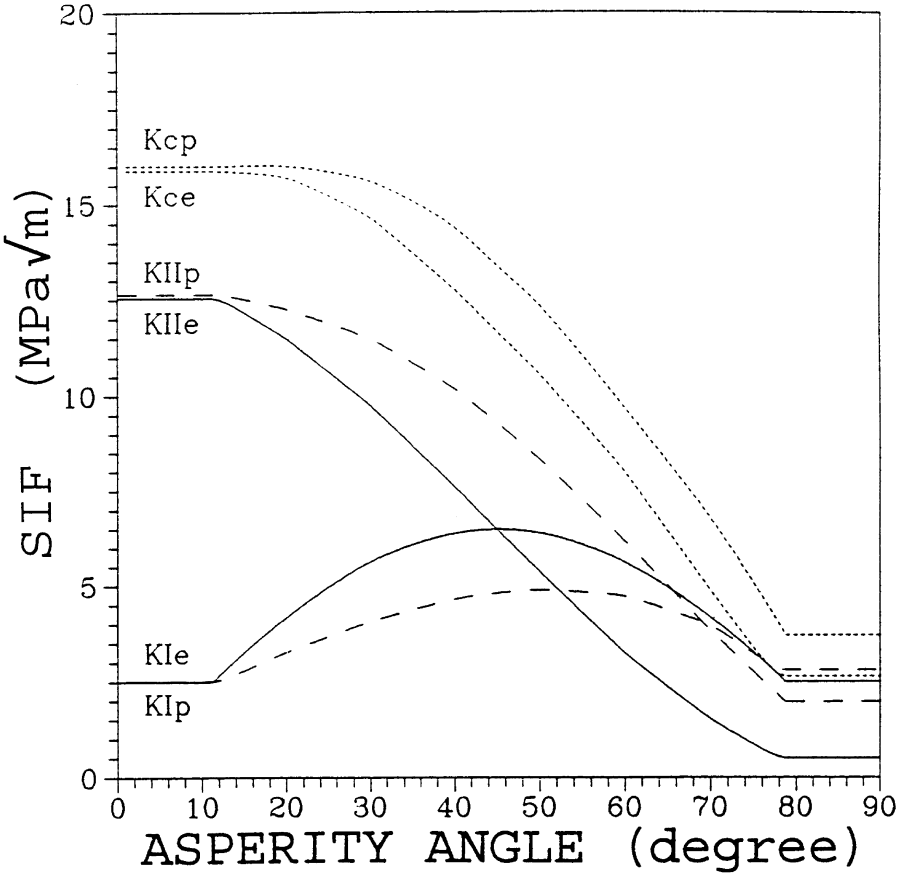

Fig. 8. Stress intensity factor vs asperity slope ($G = 80{,}000$ MPa, $v = 0.3$, $N = 20$ MPa, $S = 100$ MPa, $\mu = 0.2$, $2a = 10$ mm, $\sigma_y = 300$ MPa).

($\alpha < 11.3^\circ$), but they are not. This is due to numerical inaccuracy of the plastic case shown in Table 1 (1.89%) and the inaccuracy in the adjustment of the elastic results mentioned above.

4. BEM sawtooth model-edge crack with asperity wear

Wear can be defined as the surface damage caused by two surfaces moving past each other while in contact (Fig. 9). The asperities are assumed to begin to wear out when the macroscopic tangential resistance stress reaches the shear yield stress, as related by

$$\tau_c = \tau_y = \mu\sigma, \tag{6}$$

and

$$\tau_y = \frac{\sigma_y}{\sqrt{3}}, \tag{7}$$

Table 1
Truncation length, number of elements and accuracy of 10 mm elastic center crack in steel, with $G = 80{,}000$ MPa, $N = 0$ MPa, $S = 80$ MPa, and $\mu = 0.2$ (analytical $K_{II} = 10.03$ MPa$\sqrt{m}$)

Truncation length (mm)	Number of elements	Calculated K_I ($\sqrt{m}$)	Error %
30	30	11.84	18.05%
110	110	11.21	11.76%
190	190	11.09	10.57%
130 (plastic)	130	10.22	1.89%

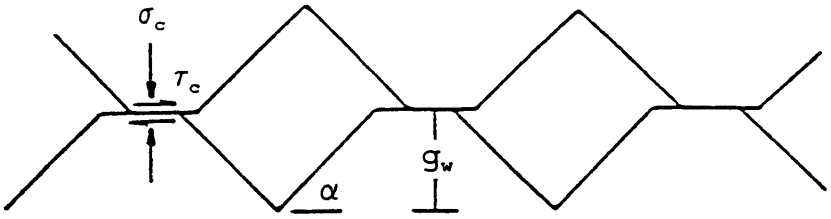

Fig. 9. Two dimensional geometry of idealized sawtooth wear with asperity angle α, crack opening displacement g_w, coefficient of friction μ.

where σ_y and τ_y are yield stress in normal and shear direction, respectively. The asperity is proposed to smear over and thereby cause a constant crack opening displacement g_w (CODW) which is the value of g (COD) at that point right before wear. The smear will be general, be an irreversible process consisting of either plastic deformation or fracture of asperities. The crack tip SIFs for elastic or plastic crack tip are calculated by the same methods as mentioned above for elastic and plastic crack tip, respectively. It seems that the crack wears totally when all asperities reach the shear yield stress, τ_y, simultaneously due to the uniformity of the applied load.

Figures 10 and 11 give the relations between K_{II}, K_I and K_{IIapp} with different asperity angles for edge crack problem (10 mm finite length crack). As in the discussion of Figs 2 and 3 for a finite crack in the infinite homogeneous body, the slopes of the K_{II} lines decrease with α everywhere, while the slopes of the K_I lines increase from 0 to 1, reach a maximum and then decrease until $\alpha = 78.69^\circ$. Once wear occurs this dependence of K_{II} on α is much less severe since the contact surface is independent of α. However, since K_I is fixed by the COD when wear occurs its post-wear value is strongly influenced by α as shown. They also show that as K_{IIapp} increases both K_{II} and K_I increase linearly. After passing the yielding point K_{II} jumps to a higher value and keeps increasing linearly. However, K_I remains the same because there are no more changes in the COD after the asperities are worn flat.

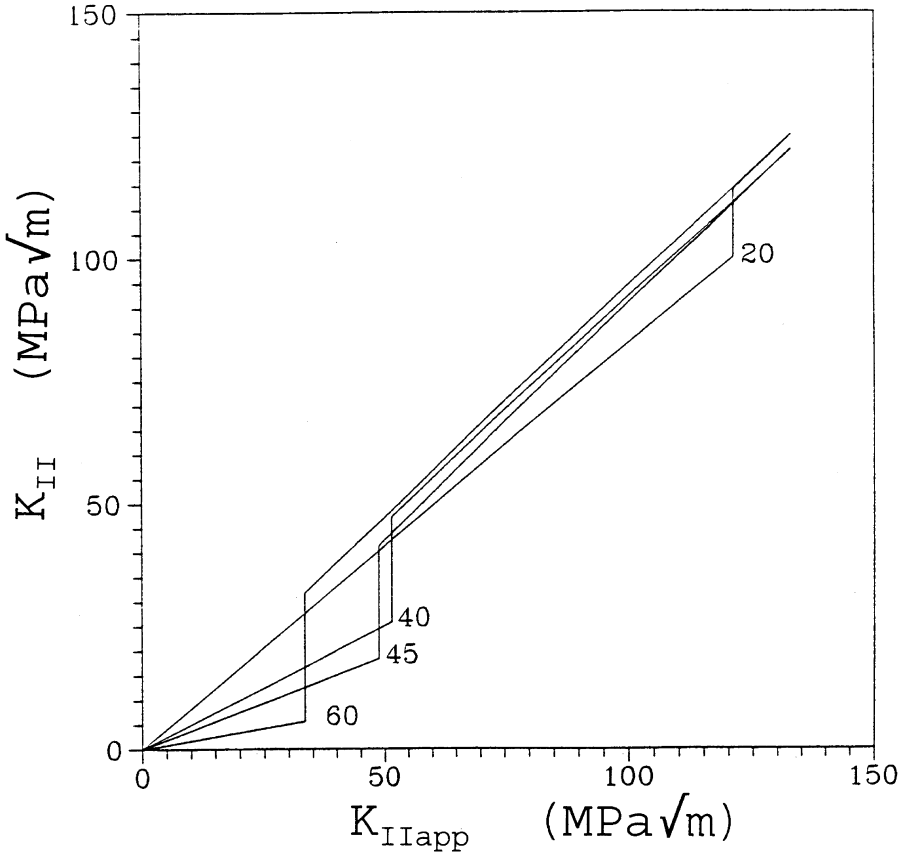

Fig. 10. K_{II} vs K_{IIapp} for various values of asperity angle α ($G = 80{,}000$ MPa, $v = 0.3$, $N = 0$ MPa, $\mu = 0.2$, $2a = 10$ mm, $\sigma_y = 300$ MPa).

5. Conclusions

A 2D elastic-plastic BEM formulation predicting the reduced mode II and the enhanced mode I stress intensity factors caused by fracture surface roughness has been presented. Three types of crack boundary conditions were investigated:

(1) DBC with elastic center crack tip.
(2) DBC with plastic center crack tip.
(3) DBC edge crack with asperity wear.

The dilatant boundary conditions (DBC) are based on the assumptions of idealized uniform sawtooth crack surface and an effective Coulomb sliding law. A simple yielding criterion for occurrence of wear and subsequent sliding on the worn asperity surface has also been presented. A re-formulation of the Dugdale plastic strip yield model has been used to analyze the results obtained by a non-linear iterative solution of the plastic crack tip of a rough DBC crack.

The BEM offers important advantages over 'domain' type solutions. One of the most interesting

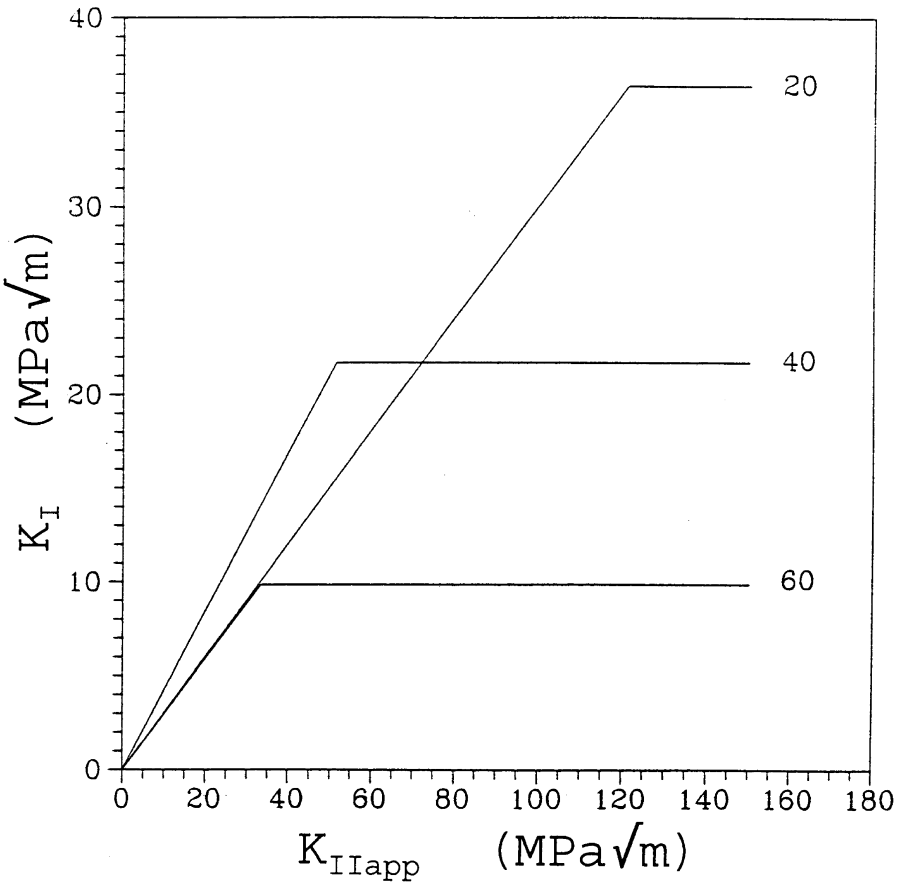

Fig. 11. K_I vs K_{IIapp} for various values of asperity angle α ($G = 80{,}000$ MPa, $\nu = 0.3$, $N = 0$ MPa, $\mu = 0.2$, $2a = 10$ mm, $\sigma_y = 300$ MPa).

features of the method is the much smaller system of equations and considerable reduction in the data required to run a problem. In addition, since conditions at infinity are incorporated in the boundary integral directly, the BEM is also well suited to problems solving with infinite domains such as the center crack problem in infinite media for which the classical domain methods are unsuitable.

Acknowledgements

This work was sponsored by National Science Council, Republic of China, through Grant NSC 87-2212-E-216-004 at Chung-Hua University and is greatly acknowledged.

References

Becker, W., Gross, D., 1989. About the Dugdale Crack under Mixed Mode Loading. Int. J. Fracture 37, 163–170.
Dugdale, D.S., 1960. Yielding of Steel Sheets Containing Slits. J. of Mech. Phys. of Solids 8, 100–108.

Erdogan, F., Sih, G.C., 1963. On the Crack Extension in Plates under Plane Loading and Transverse Shear. J. Basic Engr. 85, 519–527.

Tong, J., Yate, J.R., Brown, M.W., 1995. A Model for Sliding Mode Crack Closure, Part I: Theory for Pure Mode II Loading. Engr. Fracture Mech. 52, 599–611.

Tong, J., Yate, J.R., Brown, M.W., 1995. A Model for Sliding Mode Crack Closure, Part II: Mixed Mode I and II Loading and Application. Engr. Fracture Mech. 52, 613–623.

Young, L.J., 1994. A Boundary Element Analysis of Fracture Surface Interference for Mixed Mode Loading Problems with Elastic or Plastic Crack Tips. Ph.D. Dissertation, the Ohio State University, Columbus, Ohio, 11–38.